Received: 5 November 2022 | Revised: 24 February 2023 | Accepted: 1 March 2023

DOI: 10.1002/bte2.20220062

RESEARCH ARTICLE

BATTERY ENERGY Open Access WILEY

Cycling performance of silicon-carbon composite anodes enhanced through phosphate surface treatment

Hana T. Gobena[1] | **Samson Y. Lai**[2] | **Alexey Y. Koposov**[2,3] | **Jan P. Maehlen**[2] | **Fouad Ghamouss**[1] | **Daniel Lemordant**[1]

[1]Laboratoire Physico-chimie des Matériaux et des Electrolytes (PCM2E), EA 6368, Faculté des Sciences, Université de Tours, Tours, France

[2]Department of Battery Technology, Institute for Energy Technology (IFE), Kjeller, Norway

[3]Department of Chemistry, Center for Material Science and Nanotechnology, University of Oslo, Oslo, Norway

Correspondence
Daniel Lemordant, Laboratoire Physico-chimie des Matériaux et des Electrolytes (PCM2E), EA 6368, Faculté des Sciences, Université de Tours, Parc de Grandmont, 37200 Tours, France.
Email: daniel.lemordant@univ-tours.fr

Abstract

Silicon (Si)-based anodes have long been viewed as the next promising solution to improve the performance of modern lithium-ion batteries. However, the poor cycling stability of Si-based anodes impedes their application and calls for solutions for further improvements. In the present work, the incorporation of phosphate groups on the surface of an amorphous Si-carbon composite (a-Si/C) has been achieved by a hydrothermal reaction using phosphoric acid and sodium dihydrogen phosphate at pH = 2. Different levels of the surface P-doping have been realized using reaction times (2, 4, and 8 h) at two different phosphate concentrations. The presence of phosphate groups on the particle's surface has been confirmed by energy-dispersive X-ray, infrared, and Raman spectroscopy. The cycling stability of the P-treated a-Si/C composites has been significantly improved when using lithium bis(trifluoromethanesulfonyl)imide as a salt in ether-based solvents mixture compared to a conventional electrolyte for Si-based anodes ($LiPF_6$ in carbonate-based solvents). Coulombic efficiencies as high as 99% have been reached after five charge/discharge cycles for almost all phosphate-treated materials. The 4 h P-treated a-Si/C composite electrode exhibits the best reversible capacity of 1598 mAh g^{-1} after 200 cycles demonstrated in half-cells using an ether-based electrolyte.

KEYWORDS

amorphous silicon-carbon composite (a-Si/C), ether-based electrolytes, lithium-ion battery (LIB), phosphorus surface treatment, solid electrolyte interphase (SEI)

1 | INTRODUCTION

Lithium (Li)-ion batteries (LIBs) play a significant role in modern life and industry. They have become the main energy source for portable electronics, electric vehicles, and even for some industrial large-scale equipment. LIBs are omnipresent in multiple applications spanning from portable devices to grid-scale energy storage owing to their high energy density.[1–3] However, despite the advantages, the material set for LIBs needs to be revised to further improve their performance.

Among the potential future materials for LIB-negative electrodes, silicon (Si) appears to be one of the most promising candidates due to its high theoretical

specific capacity of 3579 mAh g^{-1} (corresponding to the formation of $Li_{15}Si_4$), which is approximately 10 times higher than that of commercial graphite (372 mAh g^{-1}, corresponding to the formation of LiC_6).[4,5] Such high capacity coupled with the low working potential of Si (0.2–0.4 V vs. Li/Li^+) leads to a very high theoretical energy density. However, the practical application of Si is severely limited by the enormous volume change (up to 300%) occurring upon Li insertion/deinsertion through cycling. Such volumetric changes result in the pulverization of Si particles, instability of the solid electrolyte interface (SEI) layer, electrolyte consumption, and finally rapid capacity fading.[6]

One of the approaches to overcome this drawback relies on downsizing of Si particles as reported by Liu et al.[7]: the decrease of the Si particle size below 150 nm eliminates fracturing during lithiation. Furthermore, the use of amorphous Si (a-Si) is another appealing pathway to enhance cyclability and stability, as a-Si, unlike crystalline Si (c-Si), does not undergo drastic restructuring upon first lithiation. However, a-Si has been less considered in the literature compared to c-Si mainly due to the wide availability of c-Si.[8,9] By using in situ electron microscopy, McDowell et al.[10] revealed that the lithiation of a-Si is kinetically favored: the average volume expansion in a-Si is lower and associated with reduced internal stress and less favorable fracture behavior as compared to c-Si. However, the large specific surface area of the nanostructured active materials may negatively affect their performance, as a large surface area will lead to the formation of a greater amount of SEI.

In Si-based electrodes, the formation of a stable SEI layer is an extreme challenge. The fracturing of Si particles leads to the appearance of "fresh" Si surfaces, leading to SEI growth and electrolyte consumption, and causes the isolation of Si particles.[11,12] In addition, even in the absence of the fracturing process, the Si particles continue to undergo significant volume changes during lithiation/delithiation. Thus, the SEI is constantly deformed and disconnected from the surface of the active material. That phenomenon leads to the continuous formation of SEI, which fills the pores of the electrode, inhibits Li^+ diffusion, and finally limits the electrode lifetime.[13–15] For instance, Radvanyi et al.[16] demonstrated the formation of a porous SEI during the initial cycles, which, however, completely fills the pores of an electrode through further cycling. As a result, Li diffusion was hampered, causing a rapid drop in capacity after several cycles. Etiemble et al.[17] also showed that the change in the electrode's porosity is primarily due to the combination of Si volume expansion and SEI growth. Moreover, Michan et al.[18] demonstrated that the capacity loss can be attributed to SEI growth and tortuosity increase.

Another approach to mitigate the challenges associated with a volume expansion of Si is coating, that is, preparation of materials with core/shell structure. Coating is the simplest approach to modify the surface of an active material to protect it from parasitic reactions with the electrolyte. Carbon-based coating is the most popular choice among various materials used for such purpose.[19] The primary advantages of carbon coating include restraining of the volume expansion by the carbon shell, while improving the electrical conductivity of Si. In addition, the direct contact of Si with the electrolyte is diminished, resulting in minimizing the aforementioned SEI challenges.[20] However, coating of Si with carbon cannot completely inhibit the volume expansion of Si, and the anode material is still subjected to a great stress during lithiation/delithiation, leading to electrode accelerated cracking and loss of contact between Si particles.[21]

Coating is also an effective approach to modify the composition and properties of the SEI and, in the most favorable cases, to increase Li-ion diffusion to facilitate the uniform expansion of the particles. Tokranov et al.[22] showed that the SEI layer formed on Si at 0.6 V is mesoporous, organic, and flexible with a high elastic modulus and tolerates the deformation associated with volume change. A second inorganic layer, formed at a lower potential (≈0.3 V), is thin and rigid and, therefore, tends to crack during cycling.[23] Similarly to particles, the performance of Si nanowires was also improved with carbon coating.[24] For instance, Chen et al. deposited a carbon layer of approximately 10 nm on Si nanowires and demonstrated that the conductive properties of this layer allowed an improvement of the high-rate charge/discharge performance. Bogart et al.[25] recently confirmed that the lithiation of carbon-coated nanowires was faster than that of uncoated nanowires by using in situ scanning electron microscopy (SEM). They also showed that the uniform carbon coating allows to restrain the volumetric changes of Si nanowires. As a result, such carbon-coated nanowires can deliver a stable capacity of 2000 mAh g^{-1} at C/10 rate for 100 charge/discharge cycles. A graphitic layer, deposited on the Si surface, can contribute to the electrode-specific capacity in addition to the protection of the active material, was reported by Cho et al.[26]

Therefore, it is clear that the surface properties of Si-based materials are critical for their performance in a battery, by controlling the overall stability of the particles and SEI formation. Herein, modification of the surface of a Si/C composite material was realized by water-based treatment using phosphoric acid with the aim to improve the performance of this material as a LIB anode by incorporating phosphate groups at the Si electrode

surface. For such modification of the Si surface, the hydrothermal method was used, which is scalable, safe, and could be performed at a low cost. The purpose of such surface modification is to generate a passivation layer at the Si surface, which will be able to limit SEI growth and achieve a more stable cycling performance.

2 | EXPERIMENTAL SECTION

2.1 | Material synthesis

The amorphous silicon (a-Si) in a form of nanoparticles, provided by the Institute for Energy Technology (IFE, Norway), was synthesized through the pyrolysis of silane gas (SiH_4).[27] As the coutilization of graphite and Si has been deemed as the most appropriate approach for the current commercial LIB system to realize high-energy density with Si anode, enabling tightly limited use of nonactive materials and mitigated volume expansion,[20] a-Si particles are mixed with graphite to obtain a Si/C composite (Si/C 4:3 by weight). Hence, graphite and silicon powders were ball milled at 200 rpm using ZrO_2 balls (ball-to-powder ratio of 5:1) for 5 min to form the Si/C composite, which was then added to 200 mL of an aqueous sodium dihydrogen phosphate (NaH_2PO_4) solution (90 or 120 g L^{-1}). The particle suspension was acidified at 40°C to pH = 2 with pure H_3PO_4 and stirred (2, 4, and 8 h) to make the Si powder more evenly dispersed. After filtration of the solution, the collected precipitate was washed with distilled water and dried using a Büchi® evaporator at 80°C for 12 h. The microstructures of the selected materials were examined by SEM (Gemini ZEISS) and energy-dispersive X-ray (EDX) analysis was performed on selected samples.

2.2 | Electrode preparation

For electrode preparation, the Si/C composite modified with dihydrogen phosphate (DHP) was used as the main active material. Sodium carboxymethyl cellulose (Na-CMC, MW = 700,000) was the binder and carbon black (CB) a conductive additive. Na-CMC and CB were purchased from Sigma-Aldrich. A buffer solution at pH = 3, consisting of citric acid and potassium hydroxide (Sigma-Aldrich), was used as a dispersant.[28,29] Preparation of the electrode slurry was carried out by adding 1 mL of distilled H_2O to 200 mg of the mixture a-Si(P)/C-CB-CMC (40:30:15:15 by wt%). The slurry was mixed using a magnetic stirrer and deposited onto a 25-μm-thick copper foil by tape casting. The electrodes were first dried at room temperature and then at 80°C under vacuum for 6 h before cell assembly. The active mass loading of the electrodes was limited to about 1.0 mg cm^{-2} to avoid accentuating the effects of volumetric expansion associated with Si lithiation. The specific capacity of the graphite is 320 mAh g^{-1} as determined by GC and that of the CB is almost negligible.

2.3 | Electrolyte preparation and cell assembly

Two different electrolytes were used for the electrochemical evaluation of the materials in the present work. The first electrolyte was an alkyl carbonate-based electrolyte containing ethylene carbonate (EC) and dimethyl carbonate (DMC) (EC-DMC, 1:1 v/v), fluoroethylene carbonate (FEC) as an additive (10% by volume) and $LiPF_6$ (1 mol L^{-1}). The second electrolyte was an ether-based electrolyte containing 1,3-dioxolane (DOL) and 1,2-dimethoxyethane (DME) (DOL-DME, 1:1 v/v) mixture (purity: 99.8%/99.5%), to which 10% FEC and Li bis(trifluoromethanesulfonyl)imide (LiTFSI, 1 mol L^{-1}) was added. LiTFSI was selected as the Li salt for DOL solutions owing to its high solubility without causing DOL polymerization and its superior thermal stability in contrast to other Li-containing salts.[30] All materials were purchased from Sigma-Aldrich, with the exception of LiTFSI (99%; from Fluorochem), and were used without additional purification. A Li metal foil was used as a counter electrode (thickness 0.38 mm, 98.9%; Sigma). GF/C-type Whatman glass microfiber filters were punched into 10-mm discs and used as separators. The amount of electrolyte added to the cell was 150–200 μL. Li|Si Swagelok-type half-cells were assembled using a-Si or a-Si-carbon composite (a-Si/C) (P-treated) electrode (10 mm in diameter), a borosilicate glass-fiber (Whatman GF/A) separator, and a Li metal foil in an Ar-filled glove box.

2.4 | Electrochemical measurement

The electrochemical measurements were performed at 25°C in the galvanostatic mode at C/10 rate with voltage cutoffs fixed at 1.5 V and 5 mV using a VMP multichannel potentiostat (BioLogic). The cycling rates are expressed as C/x, where x is the number of hours of charge or discharge. C/x rates are used all along this article as the Si mass loading of electrodes slightly varies from one cell to another within the limit indicated above. C/x rates are based on the theoretical specific capacity of Si (3579 mAh g^{-1} for $Li_{15}Si_4$): the current density for the C/10 rate corresponds to a current density of 0.25–0.30 mA cm^{-2} (electrode area: 0.785 cm^2).

3 | RESULT AND DISCUSSION

The pristine Si/C composite and samples after treatment with aqueous DHP solution (NaH_2PO_4, pH = 2, 90, or 120 g L^{-1}) for 2, 4, or 8 h were analyzed by SEM coupled with EDX, IR, and Raman spectroscopy in the wave number range of 400–3000 cm^{-1}. In the following, P-treated samples will be denoted as Si/C(PX/Y), where X and Y are, respectively, the treatment time in hours and the concentration of the phosphate solution in g L^{-1}.

3.1 | SEM and EDX observations

The modifications of the coating conditions (coating time and phosphate concentration) resulted in noticeable changes in the Si particle surface as illustrated by the SEM images displayed in Figure 1. All images demonstrate the a-Si or a-Si(P) particles of the Si/C composite electrodes. Spherical particles having average sizes of approximately 200 nm with smooth edges and a low degree of aggregation are visible in Figure 1A. No changes in the morphology of the particles are noticeable after P-treatment using a 90 g L^{-1} NaH_2PO_4 aqueous solution (SEM images not presented here) independently of the immersion time. A very slight modification of the particle surface can be seen at the largest magnification when the 120 g L^{-1} NaH_2PO_4 solution was employed for 2 h (Figure 1B) or 4 h (Figure 1C). However, a fine-grained deposit covers the surface of the particles, and the spherical shape of the particles becomes less distinct when the treatment time was extended to 8 h. In addition, small crystals could be found on the surfaces of the particles. Therefore, EDX analysis was performed on the particles to obtain more information.

The EDX analysis of the samples is displayed in Figure 2. On the pristine a-Si material (Figure 2A), the

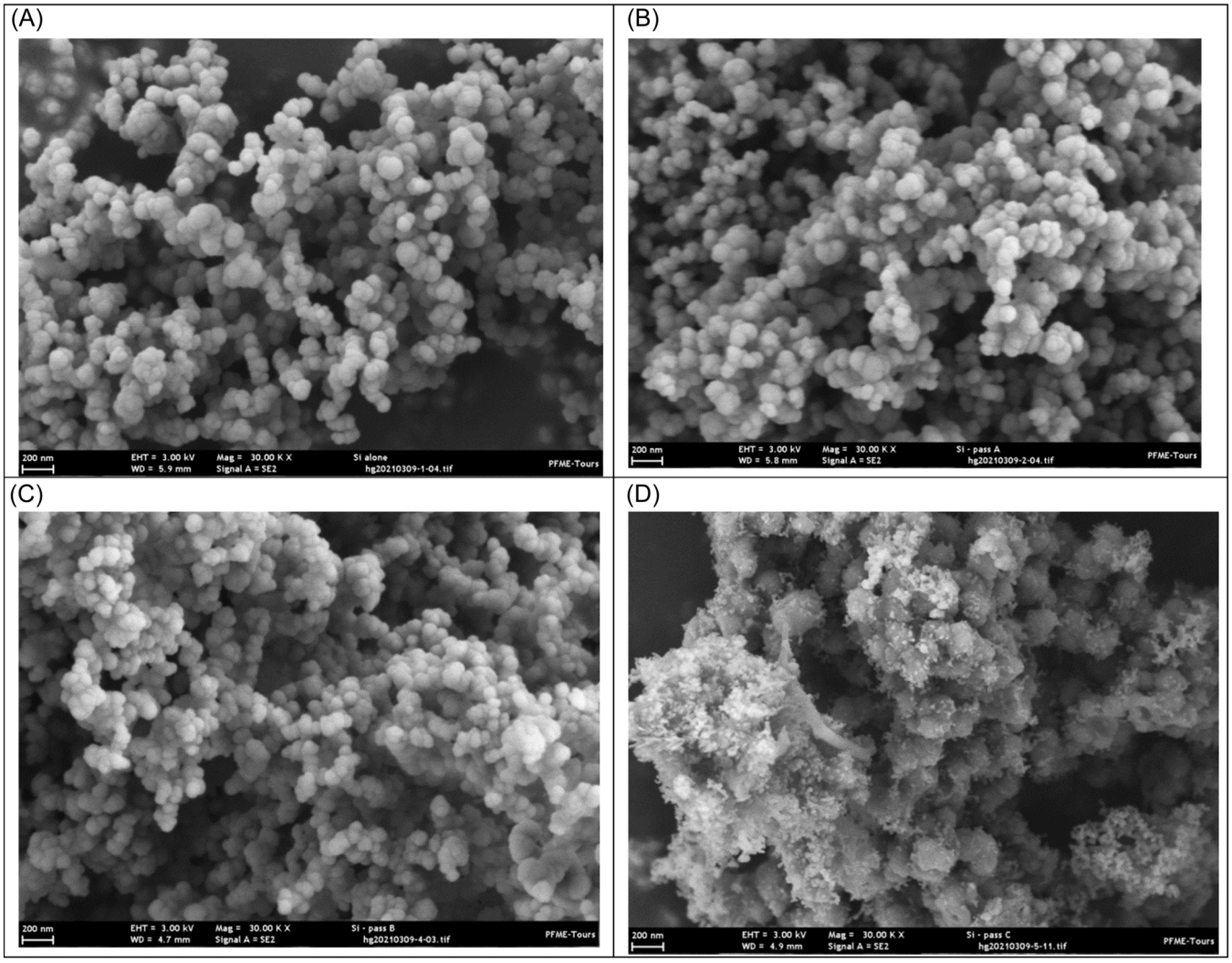

FIGURE 1 Scanning electron microscopy images of the pristine amorphous Si (a-Si) material (A), and the P-treated a-Si particles (NaH_2PO_4, 120 g L^{-1}, pH = 2) for 2 h (B), 4 h (C) and 8 h (D).

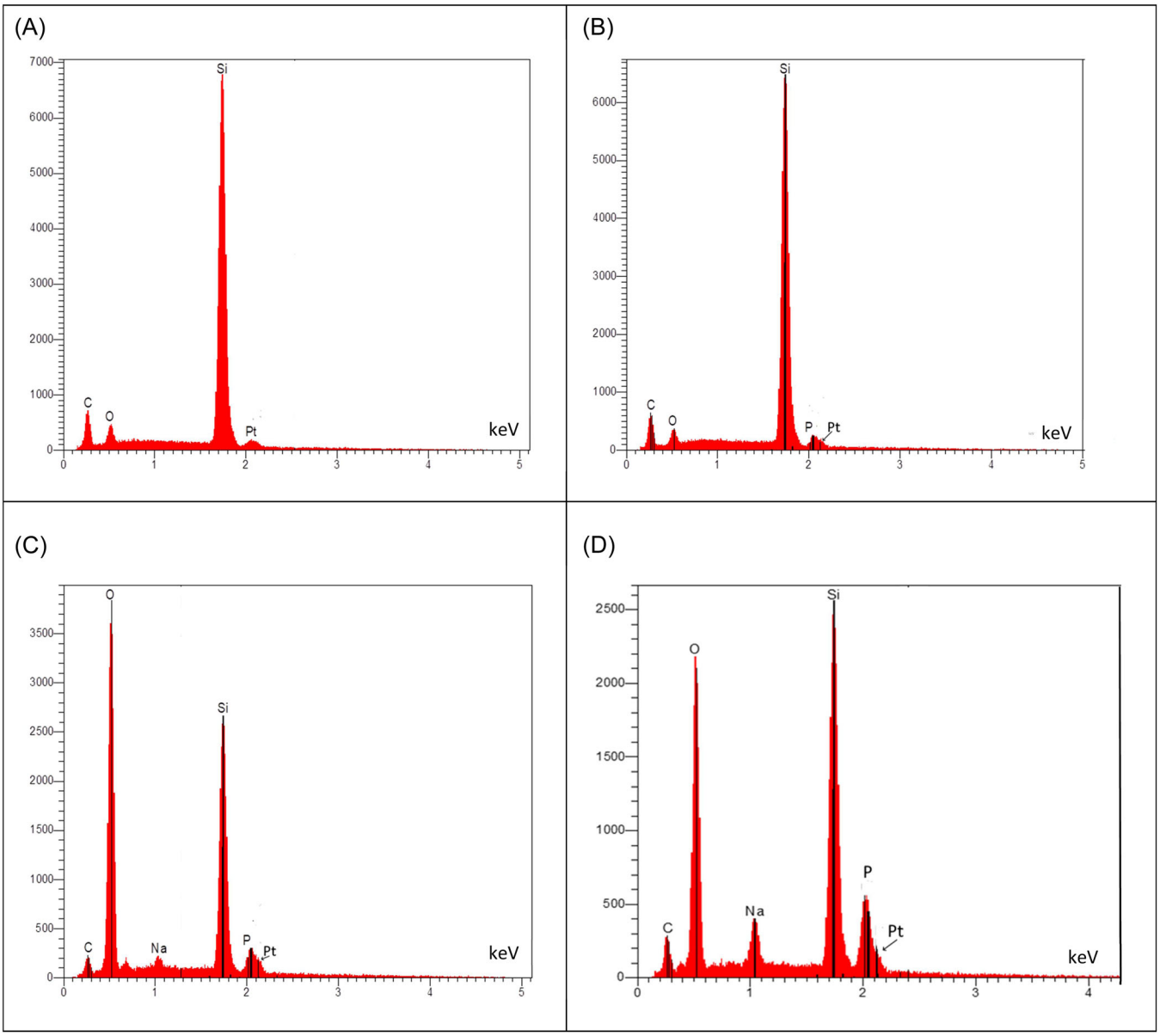

FIGURE 2 Energy-dispersive X-ray analysis of the samples presented in Figure 1: pristine amorphous Si (a-Si) material (A) and P-treated a-Si particles with NaH_2PO_4 (120 g L^{-1}, pH = 2) for 2 h (B), 4 h (C), and 8 h (D).

element C (K_α, 0.277 keV), O (K_α, 0.525 keV), Si (K_α, 1.739 keV), and Pt (M_α, 2.048 keV) are detected. C originating from the Si/C composite or CB is also presented in the electrode. Pt from the conductive coating (≈4 nm) was deposited before SEM analysis. And the O signal originates from the native SiO_2 layer, which is always presented at the surface of Si particles when exposed to the atmosphere. In Figure 2B, which illustrates an analysis of the a-Si sample treated with 120 g L^{-1} NaH_2PO_4 for 2 h, the P element peak is hardly visible at 2.014 keV ($K_{\alpha1}$) as it is mixed with the peak corresponding to Pt. When the phosphate treatment time is increased to 4 h, the presence of P becomes clearly visible as shown in Figure 2C and the Na peak is detected at 1.041 keV (K_α). In the same figure, the height of the O peak increases sharply, and this is attributed to the oxygen atoms of the phosphate groups. The presence of P, O, and Na confirms that the surface treatment is successful. With larger P-treatment times (8 h), the P and Na peaks increase strongly in height as seen in Figure 2D and the intensity of the O peak decreases, which could be due to the formation of pyrophosphate and polyphosphate by thermal condensation of sodium dihydrogenphosphate. The intensity of the O peak could be also due to the presence of NaH_2PO_4 crystals

as seen in Figure 1D, which are deposited on the particle's surface. This means that sodium orthophosphate, pyrophosphate, or even polyphosphate crystals are not completely dissolved by water during the rinsing of the sample. The a-Si treatment with the 120 g L^{-1} NaH_2PO_4 solution for 4 h is henceforth considered as the best P-treatment and used as the standard in the following studies.

3.2 | Fourier transform infrared (FTIR) spectroscopy

FTIR spectra for pristine a-Si and treated a-Si/C(P) samples are shown in Figure 3. The band observed at 471 cm^{-1} corresponds to a-Si and is followed by the peak at 620 cm^{-1} (Si-H stretching). The presence of hydrogen in a-Si particles originates from the synthesis procedure (silane pyrolysis). The band observed at 795 cm^{-1} is assigned to P-O-P stretching vibration of bridging oxygen atoms bonded to phosphorus. The vibrations at 967 cm^{-1} are assigned to the P = O terminal group. The 1156 cm^{-1} peak is attributed to Si-O-Si or Si-O-P stretching vibration with slight shifts to higher wavelengths with increased reaction time, that is, a higher concentration of phosphate on the surface. The peak at 1457 cm^{-1} is attributed to O-P-O vibration[31] originating from the P-treated SiO_2 surface layer. The presence of this peak unambiguously confirms that the surface of Si-based material has been modified with the phosphate groups. The peak at 1630 cm^{-1} is attributed to the deformation modes of O-H groups in absorbed water molecules δ(H-O-H) in a silica–phosphate nanocomposite.[28]

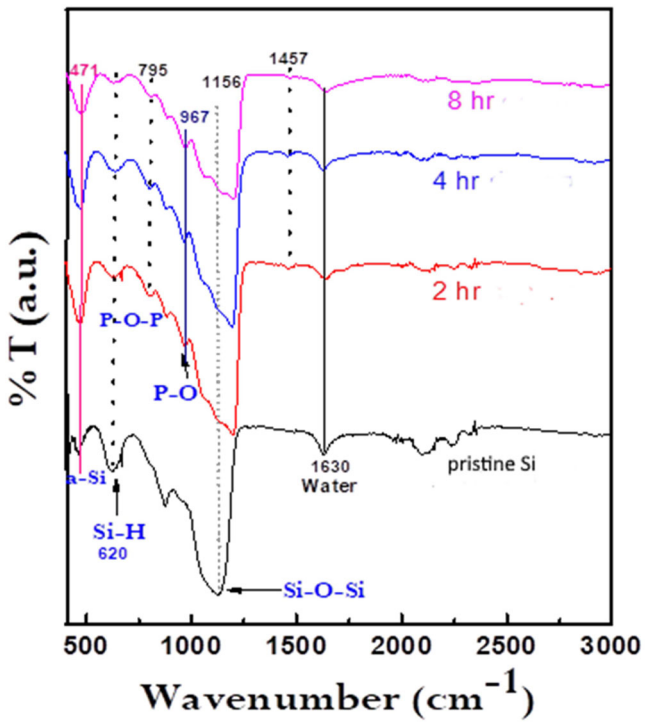

FIGURE 3 Infrared spectra of pristine amorphous Si (a-Si) (black line) and a-Si(P) after 2, 4, and 8 h treatment with 120 g L^{-1} NaH_2PO_4 at pH = 2.

3.3 | Raman spectroscopy

The Raman spectra for the pristine a-Si and a-Si/C(P) are reported in Figure 4. All samples treated with the 120 g L^{-1} NaH_2PO_4 solution demonstrated the same spectral features; thus, only the spectrum of a sample treated for 4 h is shown. Two bands around 495 and 920 cm^{-1} are visible and are assigned to a-Si and SiO_2. The standard a-SiC(P4/120) sample shows a slight peak shift to lower frequencies, which is observed for both the Si ($\delta \approx 8$ cm^{-1}) and SiO_2 ($\delta \approx 10$ cm^{-1}) vibrations. Usually, only a small shift is observed due to substitutional doping and it depends on bond lengths as well as the type of dopants. In crystalline compounds, reduction in height and asymmetry in peaks indicates lower crystallinity and improper arrangement of atoms in the lattice.[32] Figure 4 shows that the Si peak shifts to a lower wavenumber and becomes more asymmetric after NaH_2PO_4 treatment. Softening of material by heating, tensile strain, and the presence of impurities are able to shift Raman peaks toward lower wavenumber. The introduction of phosphate groups on the Si surface layer mainly composed of SiO_2 acts as an introduction of impurities, expanding the material and hence, leading to the observed frequency decrease.

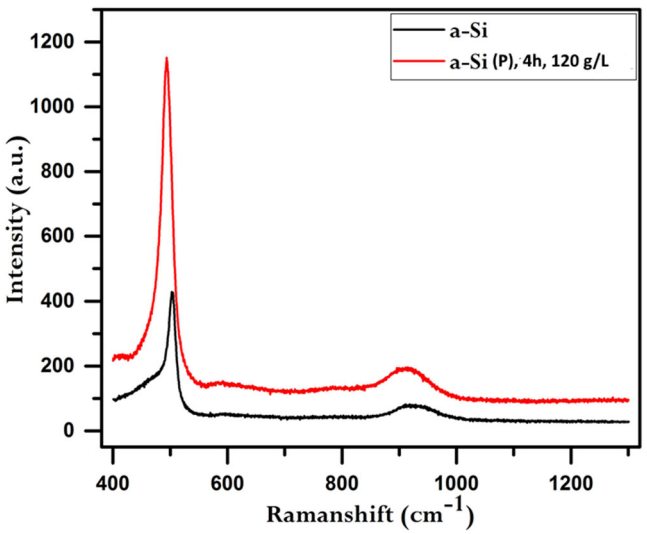

FIGURE 4 Raman spectra of pristine amorphous Si (a-Si) (black curve) and a-Si(P4/120) particles (red curve).

3.4 | Electrochemical testing

3.4.1 | CV investigation

To highlight the protective effect of the NaH_2PO_4-treated surface layer, cyclic voltammetry (CV) and galvanostatic cycling (GC) have been performed in half-cell configurations using the standard a-Si/C(P) composite as a working electrode and a Li metal foil as the reference and counter electrode. The CV curves obtained using EC-DMC and DOL-DME electrolytes are displayed in Figure 5A,B. No significant difference in electrochemical behavior between the two electrolytes was observed, except for the oxidation peak at 0.32 V, which is larger at the first reverse scan when DOL-DME was used as an electrolyte. In the first cycle, the small peak at approximately 1.65 V versus Li/Li^+ is clearly visible in Figure 5A and is related to the reduction of the FEC used as an additive.[33] As expected, this peak which contributes to the SEI formation disappears in the following cycles: it is not visible in Figure 5B as the *Y*-axis scale is at least 10 times smaller.

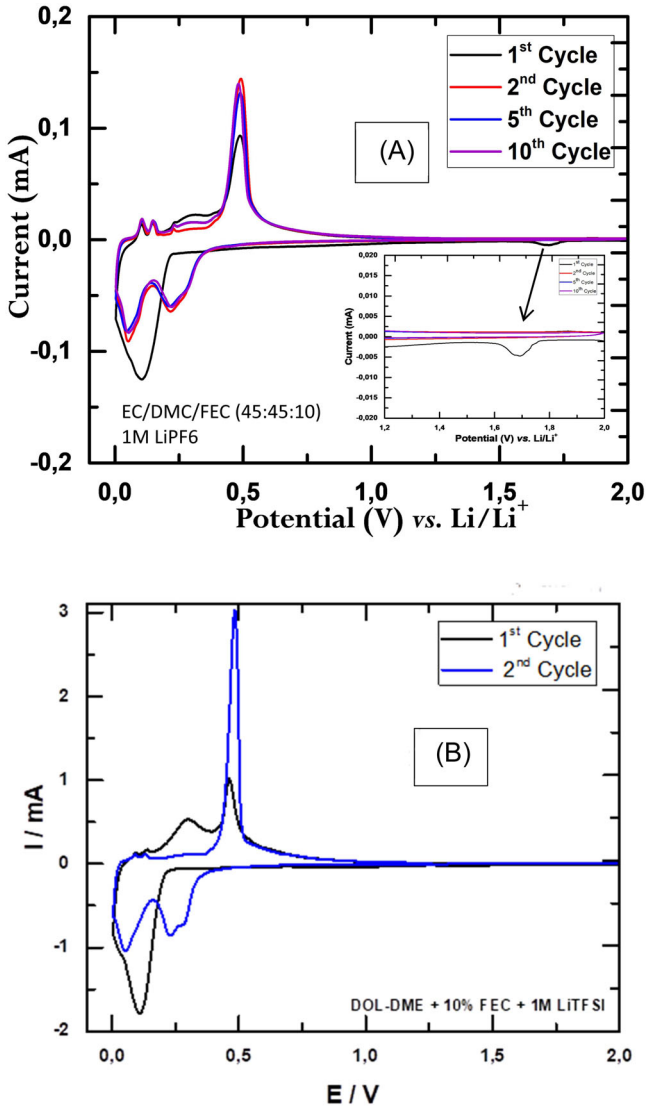

FIGURE 5 Cyclic voltammetry of standard a-Si(P4/120)/C composite anode swept from open-circuit voltage (OCV) to 5 mV versus Li/Li^+ at a sweep rate of 20 $\mu V\,s^{-1}$ in (A) $LiPF_6$ (1 mol L^{-1}) in ethylene carbonate-dimethyl carbonate-fluoroethylene carbonate (EC-DMC-FEC) (45:45:10 by vol.) and (b) Li bis (trifluoromethanesulfonyl)imide (LiTFSI) (1 mol L^{-1}) in 1,3-dioxolane-1,2-dimethoxyethane (DOL-DME) (45:45:10 by vol.). a-Si, amorphous Si.

A-Si has a higher lithiation potential (0.22 V vs. Li/Li^+) than c-Si (0.12 V vs. Li/Li^+) in the first cycle in both electrolytes. The advantage of a-Si over c-Si is that it has a higher resistance to structural fracture, which is attributed to isotropic strain/stress that restrains the particle pulverization.[15] At least five peaks are observed in the anodic direction for the standard a-Si/C(P) sample, which is attributed to the delithiation of graphite (three peaks at 0.1, 0.14, and 0.2 V vs. Li/Li^+) and to the delithiation of Si (two peaks at 0.3 and 0.5 V) as could be seen in Figure 5A,B. When the cycle number increases, the Si peak at 0.32 V decreases or even disappears, and the peak at 0.5 V, attributed to delithiation of $Li_{15}Si_4$,[34] increases. The formation of $Li_{15}Si_4$ is dictated by the voltage window selected for the present work (5 mV–1.5 V vs. Li/Li^+).

3.4.2 | GC

The electrodes prepared from standard a-Si/C(P4/120) demonstrated a high reversible specific capacity of respectively 2985 and 2270 mAh g^{-1} in DOL-DME- and EC-DMC-based electrolytes as shown by the discharge (delithiation) capacity at the first and second cycle in the galvanostatic mode (C/10 rate) illustrated in Figure 6. The irreversible capacity at the first cycle is less in DOL-DME electrolyte (710 mAh g^{-1}, i.e., 23% of the lithiation capacity) than in EC-DMC for which the irreversible capacity reached 770 mAh g^{-1} (i.e., 28% of the lithiation capacity).

The discharge capacities obtained in the subsequent cycles are reported in Figure 7 for a-Si/C and standard a-Si/C(P4/120) composite electrodes. The a-Si/C electrodes shows a drastic capacity decay in EC-DMC electrolyte at the first 10 cycles and the remaining capacity is 945 mAh g^{-1} at the 200th cycle. The capacity decay is less when DOL-DME electrolyte was used, but the capacity is only 1086 mAh g^{-1} at the 200th cycle. The standard a-Si/C(P4/120) electrode exhibits the best result in DOL-DME as the remaining capacity at the 200th cycle is 1615 mAh g^{-1} (i.e., 54% of the initial capacity). In EC-DMC the a-Si/C (P4/120) electrode exhibits a rapid decay since the 50th cycle and it is not possible to perform more than 150

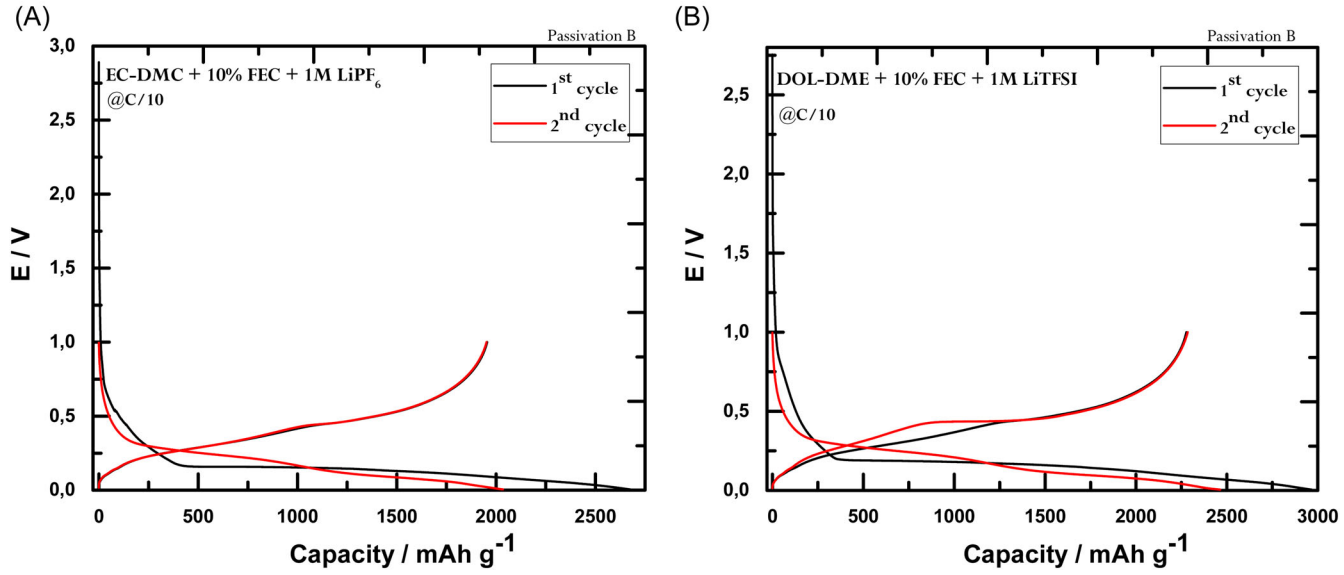

FIGURE 6 First two charge-discharge profiles of a standard a-Si(P)/C anode obtained at constant current (C/10 rate) in (A) ethylene carbonate-dimethyl carbonate-fluoroethylene carbonate (EC-DMC) and (B) 1,3-dioxolane-1,2-dimethoxyethane (DOL-DME) electrolytes. a-Si, amorphous Si-carbon composite.

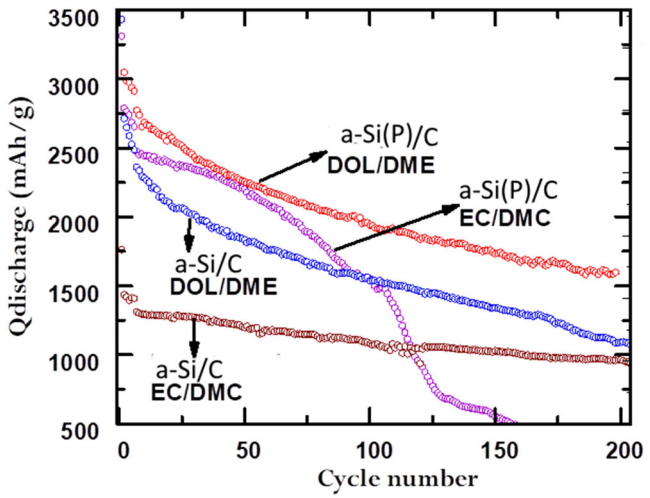

FIGURE 7 Galvanostatic discharge (lithiation) capacities versus cycle number of amorphous Si-carbon composite (a-Si/C) and a-Si/C(P4/120) electrodes in ether- and alkylcarbonate-based electrolytes between 1.5 V and 5 mV versus Li/Li+.

cycles. When EC-DMC is used as an electrolyte, the decrease of the a-Si capacity occurs in two steps exhibiting different slopes before and after about 100 cycles, and such a phenomenon has been already observed and reported.[35,36] One reason but not the sole for that could be linked to the lack of stability of $LiPF_6$, which reacts with remaining water according to the following reactions[37]:

$$LiPF_6 + H_2O \rightarrow LiF + POF_3 + 2\,HF$$

and

$$4\,HF + SiO_2 \rightarrow 2\,H_2O + SiF_4,$$

or

$$6\,HF + SiO_2 \rightarrow 2\,H_2O + H_2SiF_6,$$

where SiO_2 represents the native oxide at the silicon surface. Hence, when the SiO_2 layer is dissolved, the P-treatment becomes inefficient and the cycling performances drop, and as a result, the capacity drops to zero before the 200th cycle. On the opposite, in the ether-based electrolyte, only the $TFSI^-$ anion and FEC solvent (over 1 V vs. Li/Li^+) can be reduced as DOL and DME are hardly reducible even at 0 V versus Li/Li^+. Hence, fewer byproducts are formed in the SEI layer.

By using DOL-DME as an electrolyte, the capacity behavior is changed: it drops during the first 10 cycles and decreases slowly after. At the 200th cycle, the remaining capacity is 1100 mAh g^{-1}, which is still three times that of graphite. Using the a-Si/C(P4/120) composite, the decrease in capacity is parallel to the capacity of the untreated material, but the decrease is less during the first 10 cycles. The capacity decay trend is mainly due to the cracking of Si nanoparticles upon lithiation/delithiation cycles and the P-treatment alone is not able to prevent it. It is also important to note that this similarity only occurs in the DOL/DME electrolyte, while the trend of capacity decay is markedly dissimilar in the EC/DMC electrolyte. It is also important to note that at the 200th cycle, the capacity remains

largely higher for the a-Si/C(P) (1600 mAh g^{-1}) than for the a-Si/C composite.

3.4.3 | Effect of phosphate treatment time

Figure 8 shows the GC plots of a-Si/C(P) composites with different treatment times, in two electrolytes (EC-DMC and DOL-DME) and at various cycling rates. Figure 8A shows that a-Si(P4/120) in DOL-DME provides a better performance in long-term cycling. In contrast, Figure 8B shows that all modified samples demonstrated almost the same performance when EC-DMC was used as an electrolyte. This proves that a-Si/C(P4/120) can be cycled with almost 60% capacity retention in both electrolytes for 200 cycles and even 70% retention in DOL-DME. The initial Coulombic efficiency measured for the samples treated for 2, 4, and 8 h, when measured using DOL-DME, are 80%, 83%, and 79%, respectively, and all are stabilized above 99% after five cycles. For the EC-DMC electrolytes, the CE values are similar (Figure 8B), but one can notice that after 150 cycles, the CE is more than 100% indicating the possible formation of Li dendrites. The 4-h treatment is the best treatment time as all Si-OH groups will be converted to phosphate. Longer time will add more phosphate and polyphosphate groups at the electrode surface (by H-bonding and condensation reaction). The P-layer could then hinder Li diffusion. Moreover, the deposition of crystals at 8 h is an undesired effect.

3.4.4 | Effect of the cycling rate

To evaluate the effect of the cycling rates on the material performance, the composite electrodes have been cycled at different cycling rates between C/10 and 1C in DOL-DME and EC-DMC (Figure 8C,D). As expected, in both

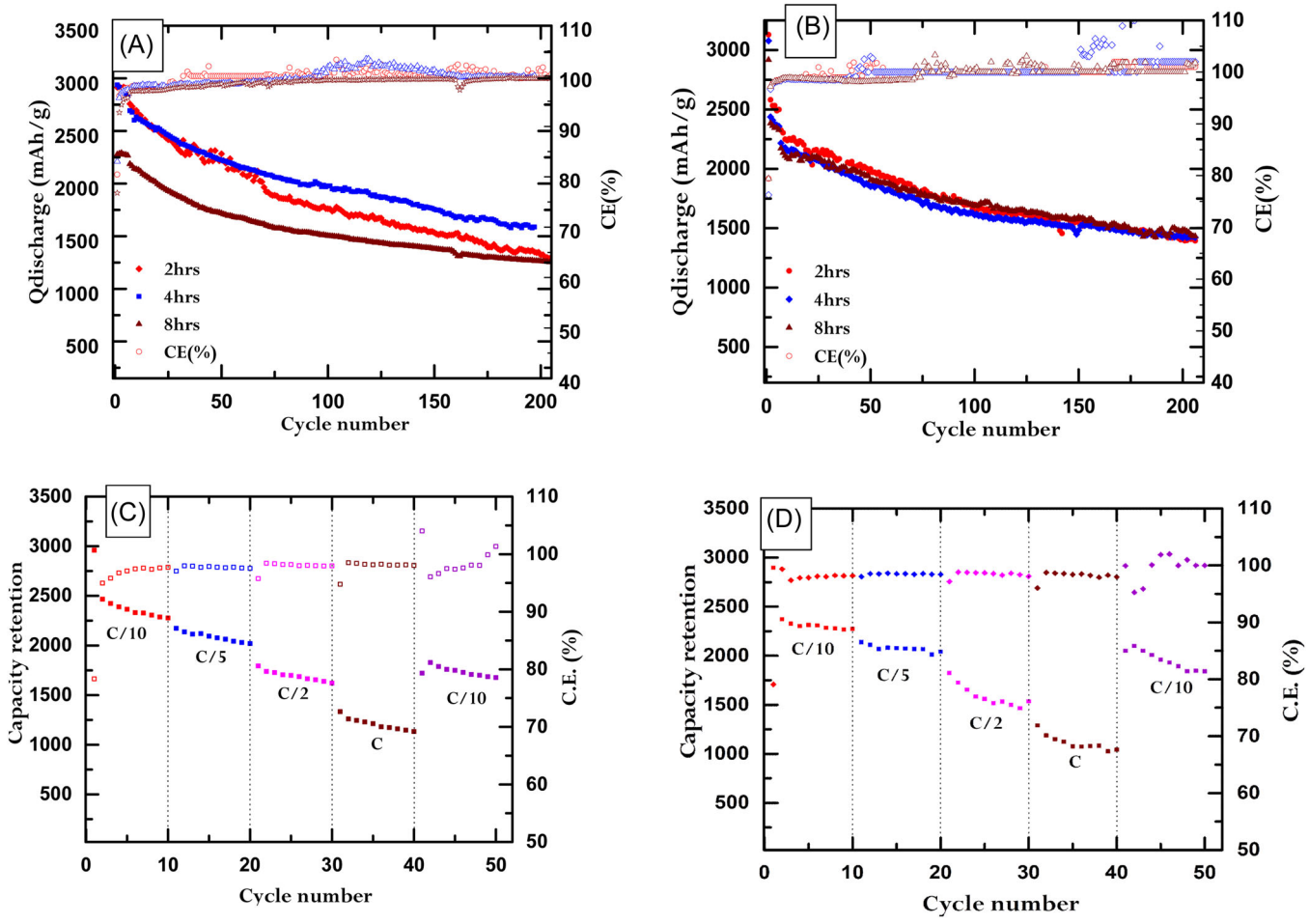

FIGURE 8 Galvanostatic charge (delithiation) capacities and C-rate effect versus cycle number of a-Si(P4/120)/C composite electrodes cycled between 1.5 and 5 mV versus Li/Li^+ in (A, C) 1,3-dioxolane-1,2-dimethoxyethane-fluoroethylene carbonate (DOL-DME-FEC) (45:45:10 by vol.) + Li bis(trifluoromethanesulfonyl)imide (LiTFSI) (1 mol L^{-1}) and (B, D) in ethylene carbonate-DMC-FEC (EC-DMC-FEC) (45:45:10 by vol.) + (1 mol L^{-1} $LiPF_6$).

electrolytes, a decrease in capacity occurs when the cycling rate is increased, but cycling at a defined rate is more stable in DOL-DME than EC-DMC. When the cycling rate is set to C/10 after 40 cycles at higher rates, the initial capacity is not fully recovered, meaning that high rates have a negative impact on the cycling stability. This could be due to Si particles becoming electrically disconnected when cycled at high rates owing to the huge volumetric change.

3.5 | DHP-treatment model

The oxide layer at the surface of Si particles is formed during exposure to air after preparation. The calculations based on the mass center position of Si layer planes show that the average thickness of each layer is equal to 0.1296 nm, corresponding to the thickness of one-half oxide layer (one oxide layer thickness is 0.26 nm).[38] The thickness of the native oxide reaches an upper limit of ~4 nm under normal atmospheric conditions, that is, about 10–15 SiO_2 layers depending upon the time, temperature, and humidity. A model of native oxide on a Si surface has been proposed by Morita et al.[39] and a schematic representation of its structure is reported in Figure 9. The Si atoms of the native oxide surface are terminated by O or OH and the Si-H groups exist at the oxide–Si interface.

In this structure, the silanol (Si-OH) groups play an important role in binding phosphate groups by means of H-bonds in the porous structure of the silica surface or at its extreme surface. Owing to the pK_a of phosphoric acid (p$K_{a1} = 2$, p$K_{a2} = 6$) and silanol (p$K_a = 5$), H-bonding due to silanol and hydrogen

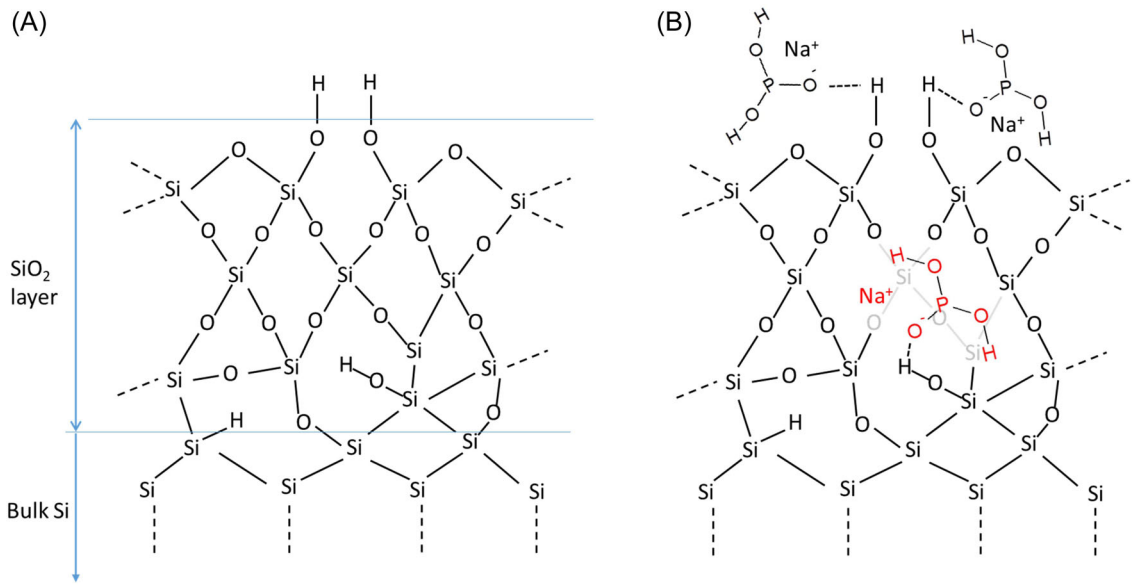

FIGURE 9 Schematic representation of the native oxide at a silicon surface grown in contact with water before (A) and after treatment (B) with NaH_2PO_4. Adapted from Morita et al.[39]

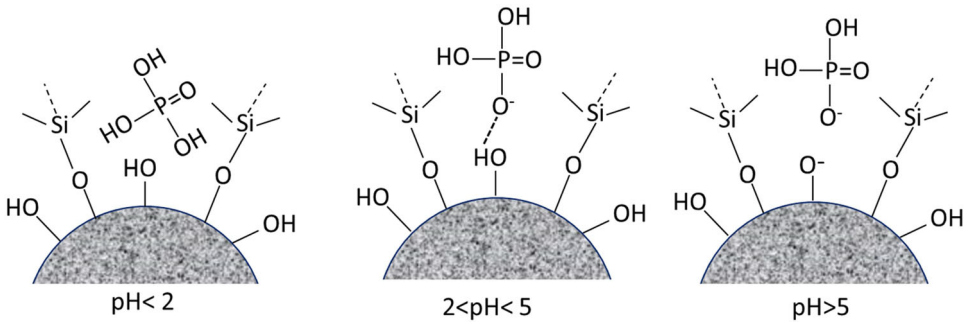

FIGURE 10 Optimum H-bonding between silanol groups and phosphate groups between pH = 2 and pH = 5. Adapted from Zhang et al.[40]

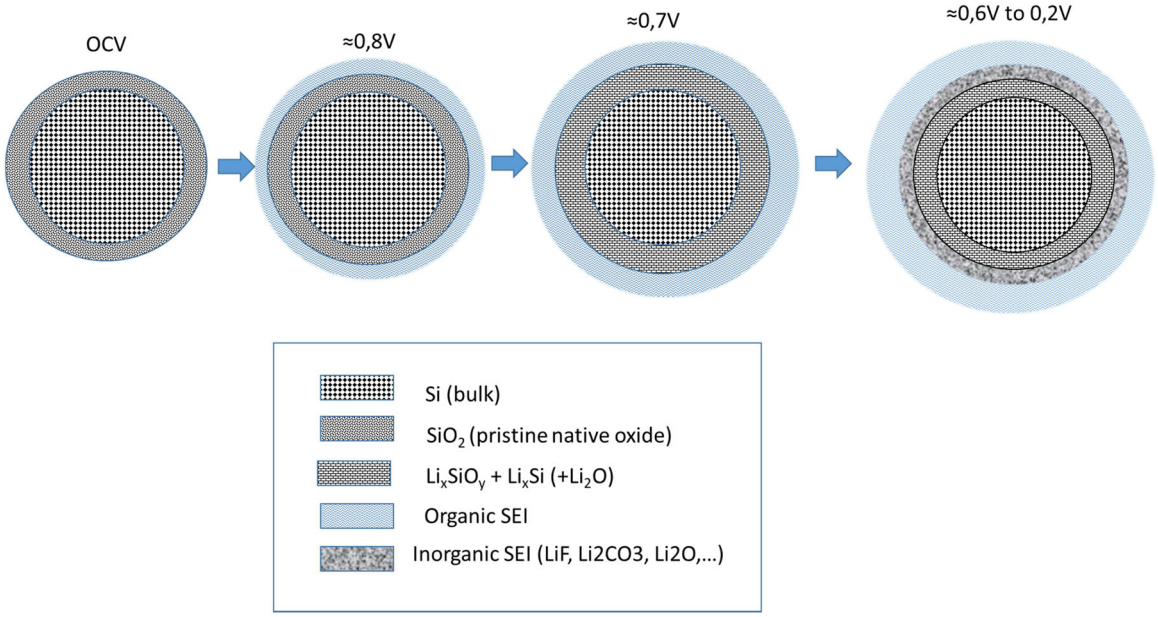

FIGURE 11 Schematic illustration of the potential-dependent solid electrolyte interphase (SEI) growth on SiOH-H_2PO_4 interphase of P-treated Si anodes from the OCV (3 V) to Li alloying at 0.2 V versus Li/Li^+. Adapted from Cao et al.[41]

TABLE 1 Cycling performances of selected Si material according to the proposed treatment.

Material	Coating or treatment	Cycle no. achieved	C (mAh g^{-1})	Current or C-rate/	Ref.
Si	Partial lithiation (70–1000 mV)	200	1000	0.36 A g^{-1}	[43]
Si/C	PHATN	500	1129.6	1 A g^{-1}	[44]
Si/C	Phosphate	200	1600	C/10	This work
Si-NP	Laser treatment	200	1000	2 A g^{-1}	[45]
Si	Si@SiO_x@C	100	1450	NA	[46]
Si	TiO_2 coating	200	1720	0.42 A g^{-1}	[5]
Si	Al_2O_3 coating	100	1921	0.26 A g^{-1}	[5]
Si	ZnO	140	1700	0.26 A g^{-1}	[5]
Si	2D-MXene	200	900	0.5 C	[5]
Si/C	Si@SiO_2@RF + TEOS	100	999.5	0.1 A g^{-1}	[47]
Si porous	LSP-Si@CNT	100	1682	0.2 A g^{-1}	[48]

Abbreviations: CNT, carbon nanotube; LSP, layered sieve-like porous silicon; NA, not available; PHATN, poly(hexaazatrinaphtalene); RF, resinol-formaldehyde; TEOS, tetraethyl-orthosilicate.

phosphate occurs in the pH range of 2–5 and a schematic view of this interaction is reported in Figure 10. The thickness of the DHP coating is approximately that of the SiO_2 layer, and the content in DHP is of the same order as the silanol groups.

DHP modification occurs on the pristine a-Si material before cycling, and hence the SEI is formed on the SiOH-H_2PO_4 layer, which acts as a Li carrier through this interphase. Volume change occurs during lithiation and delithiation processes, while DHP has no direct role in this process, the mobility of SiOH-H_2PO_4 H-bonds is able to protect the surface during expansion if limited to ca. 1500–2500 mAh g^{-1} Si. The mechanism of SEI formation on SiO_2/Si proposed by Cao et al.[41] has been adapted to the case of the a-Si (DHP) and is displayed in Figure 11. According to this mechanism, the SiOH-H_2PO_4 interphase may be reduced below 0.7 V to Li_xSiO_y and Li_xSi to form a composite Li^+ conducting mineral layer of Li_xSiO_y-Li_xSi-H_2PO_4.

4 | CONCLUSION

In the present work, we have highlighted the usefulness of DHP modification of a-Si/C composite material used as negative electrode material for LIBs. Three a-Si/C samples were treated with disodium hydrogen phosphate (90 or 120 g L^{-1}) for 2, 4, and 8 h and were used in lithium half cells to investigate the effect of this treatment on the electrochemical performance. As expected, the DHP-treated composite electrodes exhibited an enhanced cyclic performance due to the synergetic effect of the buffering matrix behavior of carbon and surface doping by DHP. The passivation of the Si surface by phosphoric acid can effectively improve the electrochemical performance in terms of capacity retention and long-term cycling. In conclusion, the best capacity retention under cycling is observed for the sample treated with phosphate (120 g L^{-1}) for 4 h and cycled in DOL-DME as an electrolyte. The reasons for the better performance in the ether mixture could be due to:

(i) the SEI formed in DOL-DME electrolyte in the presence of the FEC additive is more stable than in EC-DMC,
(ii) the use of LiTFSI as lithium salt, which does not react with water to give HF, is detrimental to the SEI and the silicon material,
(iii) the SiOH-H_2PO_4 interphase formed after DHP treatment of pristine a-Si, plays a buffering role during the volume expansion of the alloyed Si, and
(iv) the fact that DOL-based electrolytes restrain the formation of dendrites on lithium metal.[42]

As the a-Si/C(P) anode has a higher initial capacity (more than 3000 mAh g^{-1}) than the untreated material and is able to retain a capacity of 1600 mAh g^{-1} after 200 cycles in the ether-based electrolyte, this result suggests that the a-Si/C(P) material could effectively limit the formation of the SEI and mitigate the electrochemically induced mechanical pulverization of the lithiated Si, and thus, help maintain structural stability during cycling.

To compare the proposed P-treatment of the Si/C anode to other types of treatment, cycling results from the literature have been reported in Table 1.

Results reported in Table 1 show that the proposed P-treatment is able to compete with other more complex treatments in terms of cycling performance: initial capacity and residual capacity after 200 cycles. This treatment can easily be implemented on an industrial scale but the binder used must be optimized to reduce the fractionation of the particles during lithiation and delithiation cycles.[49]

AUTHOR CONTRIBUTIONS

Conceptualization: Fouad Ghamouss, Daniel Lemordant. Methodology: Hana Terefe Gobena, Fouad Ghamouss, and Daniel Lemordant. General experimental investigation and electrochemical analysis: Hana Terefe Gobena. Characterization. Raman and FTIR: Hana Terefe Gobena. Writing—original draft preparation: Hana Terefe Gobena. Writing—review and editing: Daniel Lemordant and Fouad Ghamouss. Material synthesis, funding acquisition, and reviewing: Alexey Y. Koposov, Samson Yuxiu Lai, and Jan Petter Maehlen.

ACKNOWLEDGMENTS

The authors acknowledge Dr. Pierre-Ivan Raynal for microscopy observations and EDX analysis (Plateforme IBiSA de Microscopie Electronique de l'Université de Tours). This project has been primarily funded by the Research Council within Norway's EnergiX program under grant number 280985. This work was performed within MoZEES, a Norwegian Center for Environment-friendly Energy Research (FME), cosponsored by the Research Council of Norway (project number 257653), and 40 partners from the research, industry, and the public sector.

CONFLICT OF INTEREST STATEMENT

The authors declare no conflict of interest.

DATA AVAILABILITY STATEMENT

The data that support the findings of this study are available from the corresponding author upon reasonable request.

ORCID

Daniel Lemordant http://orcid.org/0000-0001-7124-326X

REFERENCES

1. Dunn B, Kamath H, Tarascon JM. Electrical energy storage for the grid: a battery of choices. *Science*. 2011;334:928-935.
2. Kim H-J, Krishna T, Zeb K, et al. A comprehensive review of Li-ion battery materials and their recycling techniques. *Electronics*. 2020;9(7):1161.
3. Mahmud S, Rahman M, Kamruzzaman M, et al. Recent advances in lithium-ion battery materials for improved electrochemical performance: a review. *Results Eng*. 2022;15:100472.
4. Zhu S, Li H, Hu Z, Zhang Q, Zhao J, Zhang L. Research progresses on structural optimization and interfacial modification of silicon monoxide anode for lithium-ion battery. *Acta Physico Chim Sin*. 2022;38(6):2103052.
5. Liu H, Sun Q, Zhang H, et al. The application road of silicon-based anode in lithium-ion batteries: from liquid electrolyte to solid-state electrolyte. *Energy Storage Mater*. 2023;55:244-263.
6. Su X, Wu Q, Li J, et al. Silicon-based nanomaterials for lithium-ion batteries: a review. *Adv Energy Mater*. 2014;4:1300882.

7. Liu XH, Zhong L, Huang S, Mao SX, Zhu T, Huang JY. Size-dependent fracture of silicon nanoparticles during lithiation. *ACS Nano*. 2012;6(2):1522-1531.
8. Wang JW, He Y, Fan F, et al. Two-phase electrochemical lithiation in amorphous silicon. *Nano Lett*. 2013;13(2):709-715.
9. (a) Ulvestad A, Reksten AH, Andersen HF, et al. Crystallinity of silicon nanoparticles: direct influence on the electrochemical performance of lithium-ion battery anodes. *ChemElectroChem*. 2020;7(21):4349-4353; (b) Lin L, Xu X, Chu C, Majeed MK, Yang J. Mesoporous amorphous silicon: a simple synthesis of a high-rate and long-life anode material for lithium-ion batteries. *Angew Chem Int Ed*. 2016;55(45):14063-14066.
10. McDowell MT, Lee SW, Harris JT, et al. In-situ TEM of two-phase lithiation of amorphous silicon nanospheres. *Nano Lett*. 2013;13(2):758-764.
11. Choi NS, Yew KH, Lee KY, Sung M, Kim H, Kim SS. Effect of fluoroethylene carbonate additive on interfacial properties of silicon thin-film electrode. *J Power Sources*. 2006;161(2):1254-1259.
12. Liu L, Lyu J, Li T, Zhao T. Well-constructed silicon-based materials as high-performance lithium-ion battery anodes. *Nanoscale*. 2016;8(2):701-722.
13. Oumellal Y, Delpuech N, Mazouzi D, et al. The failure mechanism of nano-sized Si-based negative electrodes for lithium ion batteries. *J Mater Chem*. 2011;21(6):6201.
14. Mazouzi D, Delpuech N, Oumellal Y, et al. New insights into the silicon-based electrode's irreversibility along cycle life through simple gravimetric method. *J Power Sources*. 2012;220:180-184.
15. Delpuech N, Dupré N, Mazouzi D, et al. Correlation between irreversible capacity and electrolyte solvents degradation probed by NMR in Si-based negative electrode of Li-ion cell. *Electrochem Commun*. 2013;33:72-75.
16. Radvanyi E, Porcher W, De Vito E, Montani A, Franger S, Jouanneau Si Larbi S. Failure mechanisms of nano-silicon anodes upon cycling: an electrode porosity evolution model. *Phys Chem Chem Phys*. 2014;16:17142-17153.
17. Etiemble A, Tranchot A, Douillard T, Idrissi H, Maire E, Roué L. Evolution of the 3D microstructure of a Si-based electrode for Li-ion batteries investigated by FIB/SEM tomography. *J Electrochem Soc*. 2016;163:A1550-A1559.
18. Michan AL, Divitini G, Pell AJ, Leskes M, Ducati C, Grey CP. Solid electrolyte interphase growth and capacity loss in silicon electrodes. *J Am Chem Soc*. 2016;138:7918-7931.
19. Zhao X, Lehto V-P. Challenges and prospects of nanosized silicon anodes in lithium-ion batteries. *Nanotechnology*. 2021;32:042002.
20. Chae S, Choi S-H, Kim N, Sung J, Cho J. Integration of graphite and silicon anodes for the commercialization of high-energy lithium-ion batteries. *Angew Chem Int Ed*. 2019;59:110-135.
21. Li W, Cao K, Wang H, Liu J, Zhou L, Yao H. Carbon coating may expedite the fracture of carbon-coated silicon core shell nanoparticles during lithiation. *Nanoscale*. 2016;8:5254-5259.
22. Tokranov A, Kumar R, Li C, Minne S, Xiao X, Sheldon BW. Control and optimization of the electrochemical and mechanical properties of the solid electrolyte interphase on silicon electrodes in lithium-ion batteries. *Adv Energy Mater*. 2016;6(8):1502302.
23. Lu P, Li C, Schneider EW, Harris SJ. Chemistry, impedance, and morphology evolution in solid electrolyte interphase films during formation in lithium-ion batteries. *J Phys Chem C*. 2014;118:896-903.
24. Chen H, Dong Z, Fu Y, Yang Y. Silicon nanowires with and without carbon coating as anode materials for lithium-ion batteries. *J Solid State Electrochem*. 2010;14:1829-1834.
25. Bogart TD, Oka D, Lu X, Gu M, Wang C, Korgel BA. Lithium ion battery peformance of silicon nanowires with carbon skin. *ACS Nano*. 2014;8:915-922.
26. Cho YJ, Kim HS, Im H, et al. Nitrogen-doped graphitic layers deposited on silicon nanowires for efficient lithium-ion battery anodes. *J Phys Chem C*. 2011;115:9451-9457.
27. Lai SY, Knudsen KD, Sejersted BT, Ulvestad A, Mæhlen JP, Koposov AY. Silicon nanoparticle ensembles for lithium-ion batteries elucidated by small-angle neutron scattering. *ACS Appl Energy Mater*. 2019;2(5):3220-3227.
28. Ulvestad A, Skare MO, Foss CE, et al. Stoichiometry-controlled reversible lithiation capacity in nanostructured silicon nitrides enabled by in situ conversion reaction. *ACS Nano*. 2021;15(10):16777-16787.
29. Hernandez CR, Etiemble A, Douillard T, et al. A facile and very effective method to enhance the mechanical strength and the cyclability of Si-based electrodes for Li-ion batteries. *Adv Energy Mater*. 2018;8(6):1701787.
30. Etacheri V, Geiger U, Gofer Y, et al. Exceptional electrochemical performance of Si-nanowires in 1,3-dioxolane solutions: a surface chemical investigation. *Langmuir*. 2012;28:6175-6184.
31. Kumar P. Effect of silicon crystal size on photoluminescence appearance in porous silicon. *ISRN Nanotechnol*. 2011;2011:1-6.
32. Liu D, Flewitt PEJ. Raman measurements of stress in films and coatings. *Spectrosc Prop Inorg Organomet Compd*. 2014;45:141-177.
33. Xu C, Lindgren F, Philippe B, et al. Improved performance of the silicon anode for Li-ion batteries: understanding the surface modification mechanism of fluoroethylene carbonate as an effective electrolyte additive. *Chem Mater*. 2015;27(7):2591-2599.
34. Wetjen M, Pritzl D, Jung R, Solchenbach S, Ghadimi R, Gasteiger HA. Differentiating the degradation phenomena in silicon-graphite electrodes for lithium-ion batteries. *J Electrochem Soc*. 2017;164(12):A2840-A2852.
35. Iaboni DSM, Obrovac MN. $Li_{15}Si_4$ formation in silicon thin film negative electrodes. *J Electrochem Soc*. 2016;163(2):A255-A261.
36. Lai SY, Mæhlen JP, Preston TJ, et al. Morphology engineering of silicon nanoparticles for better performance in Li-ion battery anodes. *Nanoscale Adv*. 2020;2:5335-5342.
37. Ha Y, Stetson C, Harvey SP, et al. Effect of water concentration in $LiPF_6$-based electrolytes on the formation, evolution, and properties of the solid electrolyte interphase on Si anodes. *ACS Appl Mater Interfaces*. 2020;12(44):49563-49573.
38. Seah MP, Spencer SJ. Ultrathin SiO_2 on Si IV. Intensity measurement in XPS and deduced thickness linearity. *Surf Interface Anal*. 2003;35(6):515-524.
39. Morita M, Ohmi T, Hasegawa E, Kawakami M, Ohwada M. Growth of native oxide on a silicon surface. *J Appl Phys*. 1990;68:1272-1281.
40. Zhang J, Wang Q, Kleintop B, Raglione T. Suppression of peak tailing of phosphate prodrugs in reversed-phase liquid chromatography. *J Pharm Biomed Anal*. 2014;98:247-252.

41. Cao C, Abate II, Sivonxay E, et al. Solid electrolyte interphase on native oxide-terminated silicon anodes for Li-ion batteries. *Joule*. 2019;3:762-781.
42. Khalilov U, Neyts EC, Pourtois G, van Duin ACT. Can we control the thickness of ultrathin silica layers by hyperthermal silicon oxidation at room temperature? *J Phys Chem C*. 2011; 115(50):24839-24848.
43. Li Y, Lu B, Guo B, Song Y, Zhang J. Partial lithiation strategies for suppressing degradation of silicon composite electrodes. *Electrochim Acta*. 2019;295:778-786.
44. Wang Q, Zhu M, Chen G, et al. High-performance microsized Si anodes for lithium-ion batteries: insights into the polymer configuration conversion mechanism. *Adv Mater*. 2022; 34:2109658.
45. Zhou M, Li X, Wang B, et al. High-performance silicon battery anodes enabled by engineering graphene assemblies. *Nano Lett*. 2015;15:6222-6228.
46. Ashuri M, He Q, Shaw LL. Silicon as a potential anode material for Li-ion batteries: where size, geometry and structure matter. *Nanoscale*. 2016;8:74-103.
47. Zhang W, Li J, Guan P, et al. One-pot sol-gel synthesis of Si/C yolk-shell anodes for high performance lithium-ion batteries. *J Alloys Compd*. 2020;835:155135.
48. Ren Y, Yin X, Xiao R, et al. Layered porous silicon encapsulated in carbon nanotube cage as ultra-stable anode for lithium-ion batteries. *Chem Eng J*. 2022;431:133982.
49. Kim J, Park YK, Kim H, Jung IH. Ambidextrous polymeric binder for silicon anodes in lithium-ion batteries. *Chem Mater*. 2022;34(13):5791-5798.

How to cite this article: Gobena HT, Lai SY, Koposov AY, Maehlen JP, Ghamouss F, Lemordant D. Cycling performance of silicon-carbon composite anodes enhanced through phosphate surface treatment. *Battery Energy*. 2023;2:20220062. doi:10.1002/bte2.20220062